Journal of Electrical Bioimpedance
www.bioimpedance.net

J Electr Bioimp, vol. 1, pp. 84–92, 2010
Received: 14 Dec 2010, published: 31 Dec 2010
http://dx.doi.org/10.5617/jeb.149

Direct localised measurement of electrical resistivity profile in rat and embryonic chick retinas using a microprobe

Harsha Kasi [1,4], Robert Meissner [1], Alexandre Babalian [2,3], Harald van Lintel [1], Arnaud Bertsch [1] and Philippe Renaud [1]

1. *Microsystems Laboratory (LMIS4), Ecole Polytechnique Fédérale de Lausanne (EPFL), Lausanne, Switzerland*
2. *Ophthalmology Clinics, Geneva University Hospital, Switzerland*
3. *Unit of Physiology, Department of Medicine, University of Fribourg, Switzerland*
4. *E-mail any correspondence to: harsha.kasi@epfl.ch*

Abstract
We report an alternative technique to perform a direct and local measurement of electrical resistivities in a layered retinal tissue. Information on resistivity changes along the depth in a retina is important for modelling retinal stimulation by retinal prostheses. Existing techniques for resistivity-depth profiling have the drawbacks of a complicated experimental setup, a less localised resistivity probing and/or lower stability for measurements. We employed a flexible microprobe to measure local resistivity with bipolar impedance spectroscopy at various depths in isolated rat and chick embryo retinas for the first time. Small electrode spacing permitted high resolution measurements and the probe flexibility contributed to stable resistivity profiling. The resistivity was directly calculated based on the resistive part of the impedance measured with the Peak Resistance Frequency (PRF) methodology. The resistivity-depth profiles for both rat and chick embryo models are in accordance with previous mammalian and avian studies in literature. We demonstrate that the measured resistivity at each depth has its own PRF signature. Resistivity profiles obtained with our setup provide the basis for the construction of an electric model of the retina. This model can be used to predict variations in parameters related to retinal stimulation and especially in the design and optimisation of efficient retinal implants.

Key words: Bipolar microelectrodes, impedance spectroscopy, *ex vivo*, resistivity profiling, retina

Introduction

Millions of individuals around the world suffer vision loss due to retinal degeneration diseases such as retinitis pigmentosa and age-related macular degeneration. These diseases affect the photoreceptor cells rendering them dysfunctional and eventually causing their demise. Retinal prostheses can be used to restore some useful vision to the affected patients improving their quality of life considerably. These prostheses are based on stimulation of secondary neurons in the retina replacing the functionality of photoreceptors. Several methodologies are applied to convert visual images into a train of pulses that are transmitted to an array of electrodes positioned on the retinal surface. These pulses are then used to stimulate the viable secondary neurons. Many groups (refer to the review (1)) worldwide are working on different devices based on the placement of the implant with respect to the retina.

Neural tissue inhomogeneity is an important parameter affecting neural stimulation (2; 3). The vertebrate retina is a dense neural tissue composed of multiple layers each characterised by different cell types and densities (4) rendering it electrically inhomogeneous. By constructing an electric model based on inhomogeneity, it is feasible to compute the electric field distribution in the retina and consequently predict parameters such as threshold and resolution of stimulation for a safe and efficient retinal prosthesis. In order to construct a realistic, passive electric model of a retina, it is necessary to measure layer resistivity locally and precisely.

The resistivity of the retinal layers has been measured for various applications until now such as local electroretinograms (5) and current source density analysis (6). Researchers mainly used the four-terminal (tetrapolar) method to measure the resistivity profiles in the depth of the retina. Double-barrelled (6) and concentric (5) glass micropipettes have been employed as the pick-up electrodes previously. Tetrapolar measurements require a complicated setup due to additional electronics (such as front-end amplifier, current injection electrodes, etc.) and retina sealing issues (in *ex vivo* eyecup based experiments). These experimental setups operated in constant current injection mode creating an approximately constant current density in the measured retinal area (7; 8). During measurements, the rigid micropipettes cause a local damage to the retina allowing the perfusion solution to flow into the cleft. This could result in a local redistribution of current around the inserted micropipette that could lead to a change in measured voltage drop. This would result in an inaccurate resistivity measurement due to an increase in the current flow through the cleft leading to a higher voltage drop. In this situation, a constant current supposition results in an artificial increase in measured resistivity. Furthermore, the frequency used in previous experiments was not based on knowledge of the entire impedance spectrum. Neglecting the practical bandwidth might lead to interference of other parameters (for e.g., interface and parasitic components) on the measured signal (9). Lesser reproducibility of glass micropipettes may lead to variability in measurements (a

relatively large range of 12-16µm for electrode spacing was presented by Xu and Karwoski (10)).

In this study, an alternative and direct approach to measure local resistivities in the various layers of an isolated retina is presented. The approach uses a thin, flexible microfabricated probe of two electrodes to record impedance by an easy to setup bipolar impedance spectroscopy technique. Bipolar measurement is more suitable if one wants to measure a change at a specific position in an otherwise homogeneous sample (9). Considering each retinal layer to be homogeneous, the changes in resistivity occurring at various layer interfaces can be well detected by bipolar measurements. Our electrodes with close spacing allow high resolution resistivity profiling in relatively thin isolated rat and chick retina samples.

Materials and methods

Animals

Wistar (*Rattus norvegicus*) rats (Charles River or Janvier, France) in their postnatal period between 14 and 16 days and Lohmann race chicks (Animalco AG, Switzerland) in their embryonic stages of 12 and 18 days (E12/E18) were employed animal models in this study.

Electrode design and fabrication

Rectangular electrodes with rounded corners were used to reduce fringing effects. The dimensions and design of the microprobe used in this study is presented in Fig. 1.

The rectangular electrodes are spaced 10µm apart. The spacing between electrodes is based on a compromise between a localised measurement (high resolution) and maximum current penetration in the retina (sensitivity). Average retinal thickness for rat is 150µm (11) and chicken is 175µm (12). High resolution measurements are required to probe the different layers within the rat and embryonic chick retinas. An electrode spacing of 10µm is sufficient to obtain an elaborate resistivity profile of the retina accounting for typical retinal cell sizes ranging from 10µm. Both, an analytical (9) and finite element method based computation (Comsol Multiphysics 4.0a) of electric field penetration depth in saline (ρ=1.5Ω·m) for a 10µm spacing between electrodes revealed an approximate depth of 8.3µm (see supplementary information). The large enough penetration depth ensures probing retinal cells making an electrode spacing of 10µm appropriate for the application under consideration.

Measurement method and modelling

The choice of measurement method depends on the degree of sample homogeneity and the measurement hardware (i.e. whether the measurement hardware is better at detecting absolute or relative changes) (9). By virtue of the similarity of cells within a retinal layer, we can consider each layer to be homogeneous. Owing to their high sensitivity to small changes near the electrodes, bipolar measurements record the resistivity of the layer. Bipolar impedance measurement method is used in this study as it requires a simpler experimental setup compared to multielectrode schemes.

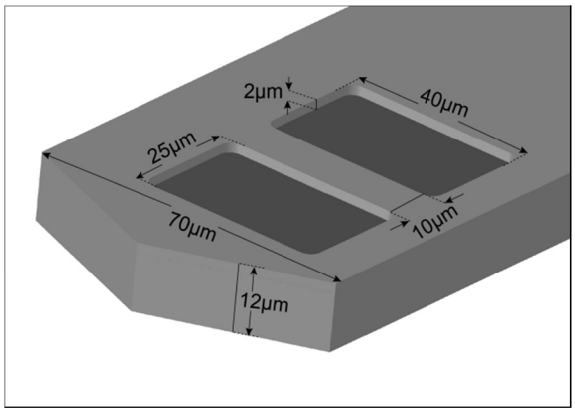

Fig. 1: A schematic of the electrodes with dimensions to scale.

The polyimide-based flexible microprobe 10-12µm thick consisted of two recessed Platinum electrodes (40µm×25µm), separated by 10µm was fabricated based on an established process (13). A photograph of the complete microprobe assembled on a plastic base for easy manipulation is shown in Fig. 2.

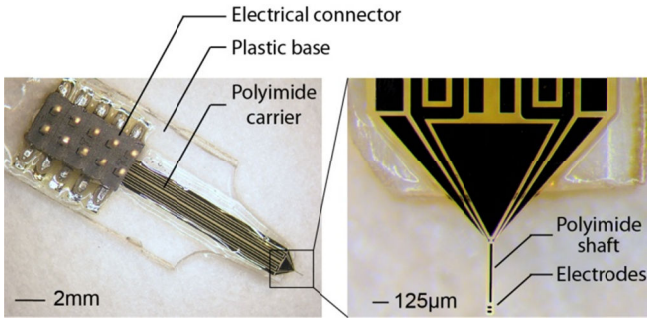

Fig. 2: Photograph of the device used. (Left) The plastic base is used to facilitate attachment to a micromanipulator (not shown) for assisting in precise insertion of the electrodes into the retina. (Right) The narrow polyimide shaft consisting of the electrodes is the part that is inserted in the retina preparation.

In order to measure a resistivity profile of the retina, it is essential to extract the resistance in each layer. For the extraction of the tissue resistance from the measured impedance, one of the approaches is to consider the impedance of an electrode-retina configuration represented by an equivalent passive electrical circuit model as shown in Fig. 3. The model consists of contributions due to the electrodes-electrolyte interface and the complex tissue impedance in series with it. The constant phase element (CPE), Z_{CPE_E} accounts for the non-ideal capacitive behaviour observed in solid metal electrodes (14). The complex tissue impedance is represented by a Cole model (15; 16) of a resistance (R_{tissue}) in parallel with a series combination of an intracellular resistance (R_{intra}) and a CPE (Z_{CPE_T}). The model is suitable for AC analysis alone.

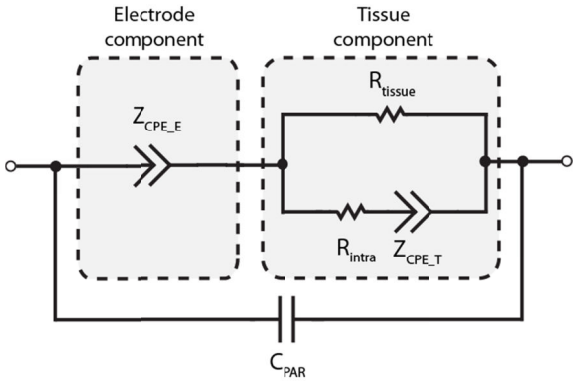

Fig. 3: An electrical equivalent representing the electrode and tissue components based on Cole model for measured tissue impedance. Z_{CPE_E} is the constant phase element (CPE) representation of the electrodes. R_{intra} is the effective resistance offered by the intracellular fluid. Z_{CPE_T} is the CPE part of the tissue impedance. R_{tissue} is the resistive part of the tissue impedance. C_{PAR} is the parasitic capacitance between the electrodes through the polyimide passivation.

A typical impedance/phase spectrum along with its model fit at a depth in the retinal tissue is presented in Fig. 4. Tissue resistance can be extracted from experimental data involving impedance/phase spectra by using fitting algorithms applied on the equivalent circuit model. Alternatively, tissue resistance has been extracted using the peak resistance frequency (PRF) method in brain tissue impedance measurements (17).

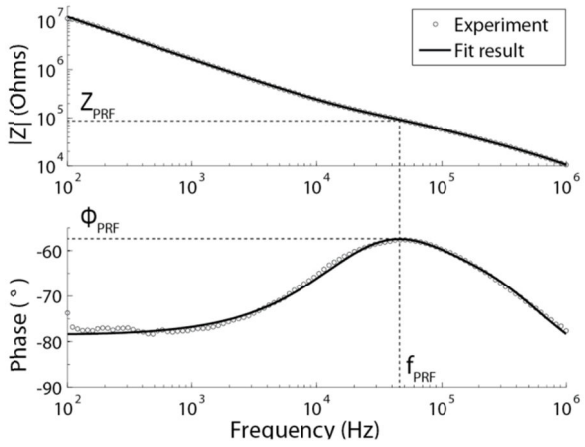

Fig. 4: Bode plot at a certain depth in the retina and the corresponding fit using the electrical equivalent. The tissue resistance is identified at the peak resistance frequency (PRF), the point at which the phase is closest to 0°.

The PRF method involves finding the frequency at which the measured impedance is least capacitive (or closest to resistive behaviour). Below this frequency, electrode CPE increases the measured impedance; above this frequency, the tissue CPE and C_{PAR} each separately or jointly decrease the measured impedance. A single choice of frequency to determine tissue resistance is usually defined by the cut-off frequency calculated from the electrode capacitance and tissue resistance itself. The PRF approach helps to define the best measurement frequency for identifying tissue resistance from a typical tissue impedance spectrum. Although, the tissue resistance can be extracted using fitting methods on the electrical equivalent (Fig. 3), its reliability is limited to uncertainties in the various fitting parameters (Z_{CPE_E}, Z_{CPE_T}, R_{tissue}, Z_{PAR}).

The tissue resistance is extracted from the impedance magnitude at the PRF. At three different depths in the retina, magnitudes at PRFs (Z_{PRF}) associated with raw experimental data compared within 10% of their corresponding fitted tissue resistance (R_{tissue}) values. We do not observe tissue relaxation as a result of the dominating electrode interface impedance (owing to the small electrode size). In view of possible misinterpretation (curbed tissue relaxation) and algorithmic errors in the fitting method using equivalent circuits, it was proposed to apply the PRF method to extract tissue resistance from impedance spectra recorded at different depths in the retina.

The resistivity (ρ) at any depth in the retina can be determined from the measured tissue resistance (R) using a simple direct relationship given by $\rho = R/k$ (18), where k is the cell constant. The cell constant of the geometry used in this study was analytically calculated as 232.75cm^{-1} according to the method described by Jacobs *et al.* (19). A 3D finite element simulation revealed a cell constant value of 232.2cm^{-1} indicating a good agreement with the analytical value (see supplementary information). The theoretical and simulated values will be used later to verify the proper functioning of fabricated electrodes. Conversion of measured electrode advance to percentage of retinal depth corrects the resistivity profiles for deviation of the microelectrodes from a plane normal to the retina and accounts for tissue shrinkage problems due to dehydration during sample preparation.

Measurement apparatus and protocol

Experimental apparatus – The experimental apparatus consisted of a three-axe Eppendorf micromanipulator 5171 used for positioning the microprobe with respect to the retina sample as shown in Fig. 5. The micromanipulator enables a uniform advancement of the electrodes into the tissue leading to a reliable impedance measurement. The extracted retina slices from a rat or embryonic chick were placed on a 3-5mm thick Agar (Sigma Aldrich, Switzerland) gel (1% in Ringer's solution[1]) inside a plastic petri-dish. The dual purpose served by Agar gel as a base for the retina is – (i) an indication for the termination of impedance measurement (low resistance of Agar gel) and (ii) a protection cushion for the penetrating electrodes preventing them from breaking by coming in contact with the petri-dish base. The petri-dish is filled with Ringer's solution submerging the retina-gel structure. All complex impedance data were acquired using an Agilent 4294A (Agilent Technologies, USA) precision impedance analyser

[1] composition (in mM) of Ringer's solution (Sigma Aldrich, Switzerland): Sodium Chloride (NaCl) – 115, Potassium Chloride (KCl) – 5, Calcium Chloride ($CaCl_2$) – 2, Sodium Bicarbonate ($NaHCO_3$) – 25, Magnesium Sulphate ($MgSO_4$) – 2, Monopotassium phosphate (KH_2PO_4) – 1 and Glucose ($C_6H_{12}O_6$) - 30

connected to a PC via a GPIB controller (National Instruments, USA). Signal frequency sweep was made from 100Hz to 1MHz for each impedance/phase spectrum, sufficiently covering the bandwidth of electrophysiological interest and ensuring the PRF is easily identified and consequently the tissue resistance. Signal amplitude of 25mV without dc offset was used as it was a good compromise between generated noise in the recorded signal and preventing possible extreme electric field effects. Moreover, it was supposed that applied signal was small enough to avoid any significant activation of retinal neurons and associated resistivity changes during measurements.

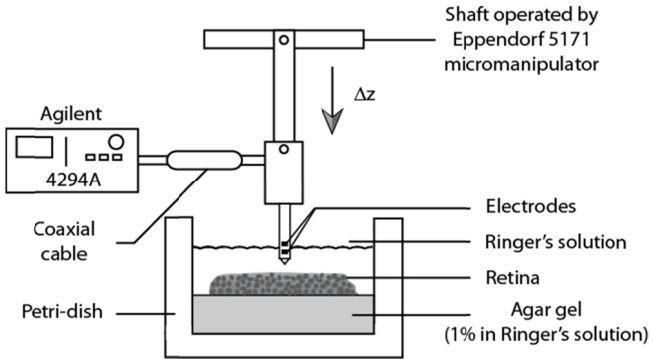

Fig. 5: Experimental apparatus consisted of (i) an Eppendorf 5171 micromanipulator that displaces the microprobe vertically (z-axis) in steps of 10μm, (ii) an Agilent 4294A impedance analyser for recording impedance/phase spectra for each probed retinal depth. (iii) a plastic petri-dish containing the isolated retinal slice placed on a block of Agar gel (1% in Ringer's solution) submerged in Ringer's solution.

Electrode cleaning and validation – Before every new experiment, the electrodes were either cleaned with 2% mild soap solution (rat trials) or chemically treated with the RCA-1 cleaning process (20) (chick embryo trials) for removing any organic contaminants. They were subsequently treated under a nitrogen gun to dry and blow away dust particles. The impedance spectrum of electrodes was obtained in standard Ringer's solution to validate their proper functioning.

Slice preparation – A common protocol for retinal slice extraction was followed for both wild-type juvenile rats and embryonic chicks. Eye balls were extracted from decapitated animals. Under low light conditions, the cornea, iris, and lens were removed from the eye ball followed by transection of the eyecup to float pieces of retina into a dish of Ringer's solution to obtain isolated retinal slices without the retinal pigment epithelium. The slices were then perfused in Ringer's solution continuously bubbled in 95% O_2/5% CO_2 until it was placed on the Agar gel. The surface on the Agar gel was pre-treated with a solution of cellulose nitrate (0.14mg/ml in methanol) and dried. This acted as an adhesion promoter for the retina to stay on the gel preventing it from being washed away when in contact with the Ringer's solution. A few moments before the experiment was conducted, the retinal slice was taken out from the perfusion and was placed on the treated area of the gel with the retinal ganglion cell side facing upwards and the photoreceptor cells in contact with the gel. The Ringer's solution was then added to fill the petri-dish to a certain level submerging the retina-gel structure.

Impedance measurement – In every trial, at least three impedance measurements at different depths (every 10μm) in the bath (Ringer's solution) before entering the retina were performed. The first considerable change in impedance magnitude at PRF indicated the entry into the retina. Visual control using a pair of binoculars confirmed this first electrode-retina contact. Subsequent impedance measurements at every 10μm depth were recorded until an impedance value similar to the one observed in the bath was encountered. Each measurement was recorded with a wait time of 30 seconds for the signal to stabilise after the micromanipulator made the 10μm vertical movement into the retina. This time was determined based on measurement of time taken for the impedance value to stabilise at a random depth in the retina (see supplementary information). Three more recordings at 10μm intervals were made to ensure the electrodes contact with the Agar gel before terminating the experiment and retracting the electrodes to the initial position. The system was under ambient laboratory conditions of 21°C during the impedance measurements.

Results

Electrode characterisation and PRF shift

To be able to compute the resistivity from the measured tissue resistance at PRF, the cell constant needs to be experimentally determined. The cell constant of the bipolar electrodes used in this study was calculated using the impedance/phase spectrum of Ringer's solution of predetermined conductivity. The spectrum is as shown in Fig. 6. Based on an average of such measurements with different batches of electrodes, an average experimental cell constant was found to be 225cm^{-1} (less than 5% error). This value is within 3.5% of the theoretical and simulated values of cell constant for the electrode configuration used in this study. The close agreement of the cell constant with previously calculated values validates the proper working of the electrodes for an experiment.

Following the functional validation of electrodes, they can be employed for impedance measurements at different depths in the retina of the chosen animal model. During these experiments, a shift in the PRF was observed at each depth in the retina as presented in Fig. 7. Starting from the retinal ganglion cell layer as we go deeper into retina towards the photoreceptor layer, the PRF moved to lower frequencies and the impedance magnitude rose from a low to a high value between 80-85% of retinal depth spanned during the experiment. With reference to Fig. 7, a 10% retinal depth corresponded to an approximate microprobe displacement of 14μm in the rat retina.

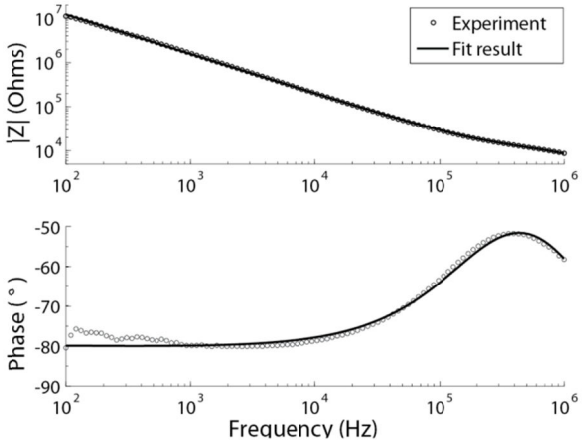

Fig. 6: Bode plot in Ringer's solution and the corresponding fit using the electrical equivalent replacing the tissue component by a simple resistor representing the solution resistance. The solution resistance is extracted from the modified model fit. Knowing the resistivity of the medium, an experimental cell constant of 225cm^{-1} was calculated. From fitting, the magnitude of Z_{CPE_E} was found to be $3.154\times10^{-10}\ \Omega^{\alpha-1}\cdot F^{\alpha}$, where α=0.85.

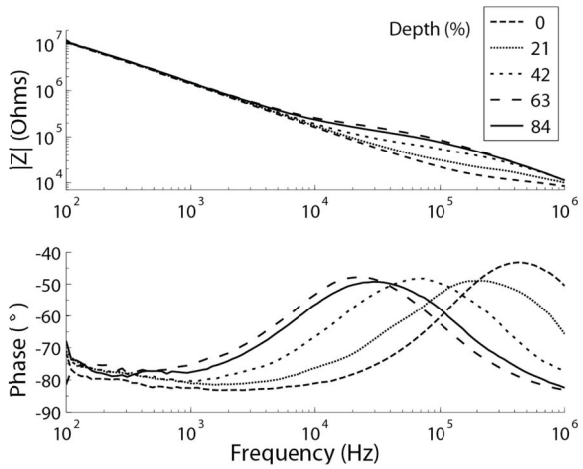

Fig. 7: PRF shift observed at various depths in a rat retina. As the PRF shifts from the right to left, the impedance increases with increasing depth into the retina (from the retinal ganglion cell towards photoreceptor layer). Depth is normalised to 100% retinal depth. A 10% retinal depth corresponded to an approximate microprobe displacement of 14μm in the retina

Resistivity profiling in rat and embryonic chick retinas

Impedance spectroscopic measurements at different depths of isolated retinal slices from three rat (14-16 days postnatal) and five chick (three E18 and two E12 embryos) samples were performed. Resistivity values were calculated from the extracted impedance value at the PRF using the direct relation between both for each depth in the retina sample. A resistivity depth of 100% was denoted as the last measurement in the retina before an identical value of resistivity obtained in Ringer's solution is reached (electrodes in Agar gel). Point zero represented the last measurement in the Ringer's solution before there is a significant change in the resistivity, i.e., an appreciable shift in the PRF is observed. Resistivity versus retinal depth profiles for both rats and embryonic chicks are presented in Fig. 8 and Fig. 10 respectively.

In both rat (Fig. 8) and embryonic chick (Fig. 10) measurements, an increasing resistivity-depth profile is observed rising gradually from the retinal ganglion cell layer towards the photoreceptor layer. At an approximate depth of 65%, the resistivity reaches a maximum value and then gradually decreases to attain a value obtained in Agar gel. There is a close interspecies resemblance in the studied resistivity profile shapes.

The maximum mean resistivity reached in rat retina samples is 4.2 ± 0.9 Ω·m and for E12 chick is 4.5 ± 0.2 Ω·m occurring between 65-70% retinal depths. On the other hand, the maximum mean resistivity in E18 chick retina samples is 7.9 ± 0.6 Ω·m which is approximately double the value measured in rats and E12 chicks at the same retinal depth. In rat and E18 chick resistivity profile measurements, at around 80% depth into the retina, there is a definite dip in the resistivity profile gradually decreasing into a low value similar to a measurement in Ringer's solution.

The standard deviation (SD) of resistivity from the mean resistivity value at each depth was examined. For the embryonic chick resistivity profiles, it is determined that the SD is low in the Ringer's solution and the Agar gel. In contrast, the rat data demonstrates large SD in these two regions of the resistivity profile.

It is known that there is a PRF shift with a resistivity change in different retinal layers. A representation of the relationship between PRF and resistivity based on the experiments on rat and embryonic chick retinal slices is depicted in Fig. 9 and Fig. 11 respectively. The log resistivity is linearly dependent on the log PRF for both the species. For embryonic chicks, owing to similarity in the data across various trials, it can be observed that there is a unique PRF for each resistivity. On the contrary, the three rat trials suggest multiple PRFs for each resistivity.

Discussion

To the best of our knowledge, planar, bipolar microelectrodes on a flexible substrate were used for the first time in this study to measure resistivity-depth profiles in rat and embryonic chick retinas. We first demonstrated the functionality of the microfabricated device. The electrode cell constant extracted from the measured solution resistance in Ringer's solution compares well with the value obtained by equivalent circuit fitting. The resistivity values at different depths in the retina established by the PRF method are within 10% of the fitted values. This is a confirmation of the electrode interface impedance not interfering with the measurements. There was a close agreement between the experimental and the theoretical/simulated bipolar cell constant values. The experimental value of 225cm^{-1} is low compared to the combined average of both theoretical and simulated value of 232.5cm^{-1}. This low difference of 3.5% is within the experimental variations. Hence, the rounded corners of the

electrodes instead of sharp perpendicular shapes may have contributed to reduction in fringing effects of electric field originating from the electrode edges. The resistivity-depth profiles, in both rat and embryonic chick experiments, indicate the inhomogeneous nature of the retina and the trend they follow are in accordance with the results obtained for various species in previous studies (5; 6). This confirms that our method is valid for retina resistivity profiling studies.

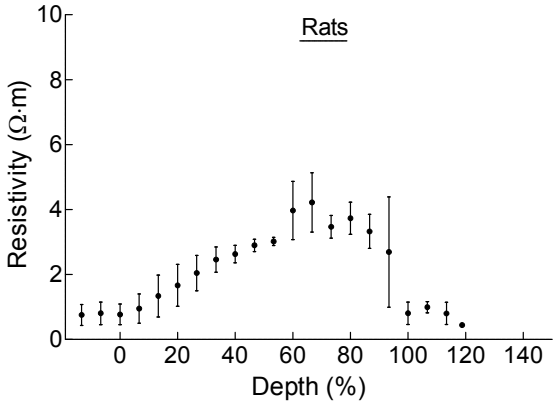

Fig. 8: Mean resistivity (±SD) vs. percentage depth profile of three rat retina samples which are extracted from 14-16 day old postnatal wild-type juvenile rats.

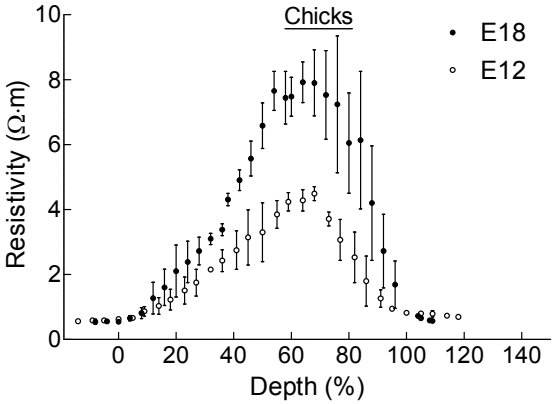

Fig. 10: Mean resistivity (±SD) vs. percentage depth profile of five chick embryo retina samples of which three are extracted from E18 and two from E12. E18 have a higher peak mean resistivity than the E12 chick trials.

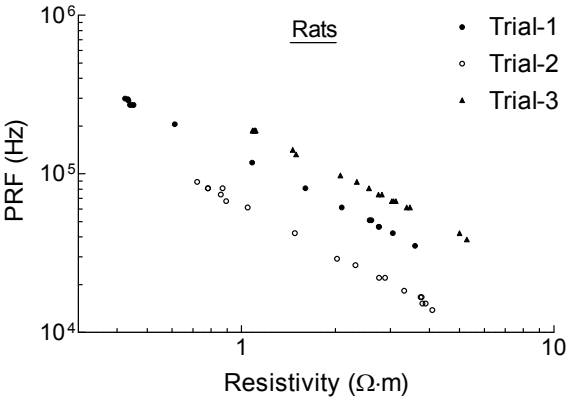

Fig. 9: PRF vs. resistivity plots for the three rat experiment trials. A large deviation for resistivity at a particular PRF between the trials was observed.

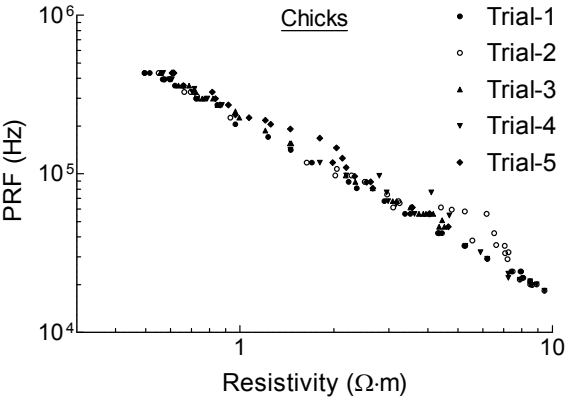

Fig. 11: PRF vs. resistivity plots for the five embryonic chick trials. In general, a good reproducibility of resistivities at a particular PRF in the trials was observed.

We found the maximum local resistivity occurred in all experiments between 65-70% retinal depths. This can be explained by greater retinal resistivity in regions like the inner nuclear layer (INL) where neurons are packed more tightly than the inner plexiform layer (IPL) (7). Our observations are in close agreement with the local maxima occurring at retinal depths of ~80% in monkey (5), ~75-80% in rat (21) and ~70% in chicken (7). The shape of the resistivity profile of the chick embryo was similar to that of the chicken (7) and the rat resembled mammalian species (5) to a large extent. This was particularly true in the region between the proximal retina and down to the junction of inner and outer photoreceptor segments. We observed an appreciable dip in the resistivity values from a retinal depth of 80% onwards until electrodes come in contact with the Agar gel. This decrease in resistivity in the photoreceptor layer was also found in previous studies using isolated slice models of avian (7) and rat (21) retinas. The local decrease in resistivity might be caused by the relatively large interstitial spaces among the outer and inner receptor segments (21). Resistivity profiles are affected by the type of retinal preparation used (isolated retinal slices and eyecup preparations). For comparing profiles, the anatomical difference between an isolated slice and an eyecup preparation of retina needs to be considered owing to the absence of the retinal pigment epithelium. In an isolated slice preparation, considering that photoreceptors offer low resistance, the effective resistivity profiling is made between the inner and outer limiting membrane (22).

We observed higher resistivity values in E18 compared to E12 chicks. This can be attributed to the ongoing retinogenesis which terminates only at E18 (23). Cell differentiation between E12 and E18 is accompanied by cell polarization, laminar stratification and changes in cell numbers (23; 24) potentially accounting for resistivity

changes within the retina. Further exploration of this subject can be interesting for future studies.

The absolute resistivities found in this study are lower compared to previous findings in rats (21) and chicken (7). The values may be difficult to compare with former investigations as the measurements are influenced by various factors like the interracial difference, age difference, measurement technique, electrodes used, etc. A majority of previous studies used the tetrapolar method with a constant current injection. The local damage caused by the pick-up micropipettes in the retina may cause a local current increase due to inflow of the perfusion solution. This could lead to an increased voltage drop resulting in a false increase of measured resistivity. In addition, most of the studies were conducted in the low frequency region (ranging between 1Hz and 100Hz) with very small electrodes (~2-20μm) (5; 6; 25). Regardless of the method used, *i.e.* bipolar or tetrapolar, it is critical to observe the whole impedance spectrum to identify the practical measurement bandwidth (9).

The maximum SDs from the mean resistivity at certain retinal depths in our study was found to be high. A large variability between trials was also observed in previous studies of rat and chicken (7; 21) that were used for comparison to our findings. All measurement techniques until now including ours have the following inherent drawbacks that affect the resistivity-depth profiling of the retina – (i) the movement of the electrode relative to the tissue not being accurate due to chip-tissue slippages, (ii) pressure causing damage to the tissue (iii) damage to the tissue by electrodes causing a high-current shunting between them resulting in an erroneous measurement of resistivity in the retinal layers and (iv) unpredictability of resistivity values at the retinal layer boundaries. Apart from these factors, the location on the retinal slice where the electrodes penetrate is a significant reason for the variability in resistivity measurements. A solution, even though it contributes to the experimental complexity, may be to locally stain the retina as a visual aid for electrodes insertion to produce reproducible resistivity profiles of the retina.

The small electrode spacing of the bipolar electrodes permitted high resolution measurements in rat and embryonic chick retinas. The high resolution profiling consisted of 25 depths in embryonic chicks and 15 depths in rats. Assuming a 10μm microprobe displacement into the retina, the 10μm spacing between the electrodes used in our study is more sensitive to capture the subtle changes in resistivity between the layers. Previous investigations employed larger electrode spacing of ~25μm (5) and ~12-16μm (6). Our electrodes design is an improvement in terms of measurement resolution compared to literature.

An important result of our study is that the resistivity at a certain depth within the retina is identified by a unique PRF in embryonic chick experiments. Conversely, distinct profiles (refer Fig. 9) were obtained in the PRF versus resistivity plots for rats. These profiles can be understood based on the large SDs observed in the Ringer's solution before entering the retina and in the Agar gel (refer Fig. 8). Although the PRF is the frequency at which the measured impedance is most resistive, representing the tissue resistance, it is influenced by interface and parasitic capacitances. The large differences in resistivities observed for calibrated mediums could be attributed to changes in electrode capacitance. This may be perceived as the electrodes not being sufficiently clean before the experiment. There could be a thin layer of adsorbed proteins from the retinal tissue cells or damaged limiting membrane residues that may add to the overall measured impedance. Electrodes were cleaned with mild soap solution for rat experiments whereas with RCA-1 cleaning procedure for the embryonic chick experiments. Thus, we conclude that quality of an electrode surface is crucial for good resistivity profiling in a retina and RCA-1 cleaning process is more effective compared to soap for electrodes used in this study.

Conclusion and future work

An alternative method for high resolution resistivity profiling along the depth in a retina based on bipolar impedance spectroscopy was established. We validated our device by profiling rat and embryonic chick retinas. The resistivity at each retinal depth was calculated based on tissue resistance extracted by peak resistance frequency methodology. Qualitatively, we found the resistivity-depth profiles to be in accordance with earlier studies and that resistivity at any arbitrary retinal depth is characterised by a unique peak resistance frequency. We have shown the potential of planar bipolar microelectrodes as a new technique to probe absolute local resistivity within a retina and multi-layered tissues, in general.

Determining absolute values of resistivities in retina contributes to improved understanding of retinal stimulation by means of modelling studies. The generated resistivity profiles can form the basis for construction of a realistic electric model of a retina. Finite element modelling may be used for estimating and optimising critical parameters such as stimulation thresholds, heat dissipation, resolution, etc. for a given electrode geometry, that are instrumental for the safety and efficacy of a retinal prosthesis. A future improvement of our two-electrode system would be a linear array of electrodes on a single strip. An array of electrodes is capable of probing different layer resistivities with a single insertion into the retina which is expected to cause less damage and provide more reliable measurements.

Acknowledgements

The authors wish to thank S. Muralidhar and V. Delattre, Neural Microcircuitry Laboratory (LNMC) for their assistance with fresh rat retinal slice preparations; A. Mercanzini, T. Braschler and W. Hasenkamp,

Microsystems Laboratory (LMIS4), in Ecole Polytechnique Fédérale de Lausanne (EPFL) for their assistance in resolving experimental issues. Our valuable discussions with Dr. F. Chiodini (University Eye Clinic, Geneva) were greatly appreciated. We are grateful to Dr. J. Patterson for the generous and timely supply of chick eggs complemented by useful tips; Prof. A.-G. Botton for the guidance and excellent incubation facility offered at the Life Sciences (SV) in EPFL. This study was financially supported by the Swiss National Science Foundation research project 315200-114152. The authors especially appreciated the timely effort of the reviewers and contribution of the editor to the rapid issue of this paper.

References

1. Chader GJ, Weiland J, Humayun MS. Artificial vision: needs, functioning, and testing of a retinal electronic prosthesis. [Internet]. Progress in brain research. 2009 Jan ;175(09):317-332.Available from: http://www.ncbi.nlm.nih.gov/pubmed/19660665
2. Lee DC, Grill WM. Polarization of a spherical cell in a nonuniform extracellular electric field. [Internet]. Annals of biomedical engineering. 2005 May ;33(5):603-15.Available from: http://www.ncbi.nlm.nih.gov/pubmed/15981861
3. Miranda PC, Correia L, Salvador R, Basser PJ. Tissue heterogeneity as a mechanism for localized neural stimulation by applied electric fields. [Internet]. Physics in medicine and biology. 2007 ;52(18):5603-17.Available from: http://www.ncbi.nlm.nih.gov/pubmed/17804884
4. Rodieck RW. The Vertebrate Retina: Principles of Structure and Function, Pg. 781. W.H.Freeman & Co Ltd (October 24, 1974); 1973.
5. Heynen H, Norren D van. Origin of the electroretinogram in the intact macaque eye--II. Current source-density analysis. [Internet]. Vision research. 1985 Jan ;25(5):709-15.Available from: http://www.ncbi.nlm.nih.gov/pubmed/4024471
6. Karwoski CJ, Xu X. Current source-density analysis of light-evoked field potentials in rabbit retina. [Internet]. Visual neuroscience. 1999 ;16(2):369-377.Available from: http://www.ncbi.nlm.nih.gov/pubmed/10367970
7. Ogden TE, Ito H. Avian retina. II. An evaluation of retinal electrical anisotropy. [Internet]. Journal of neurophysiology. 1971 May ;34(3):367-373.Available from: http://www.ncbi.nlm.nih.gov/pubmed/5560038
8. Karwoski CJ, Xu X, Yu H. Current-source density analysis of the electroretinogram of the frog: methodological issues and origin of components. [Internet]. Journal of the Optical Society of America. A, Optics, image science, and vision. 1996 Mar ;13(3):549-556.Available from: http://www.ncbi.nlm.nih.gov/pubmed/8627411
9. Linderholm P. Two-dimensional microimpedance imaging for cell culture monitoring. PhD thesis. 2006 ;234 pages.
10. Xu X, Karwoski CJ. Current source density (CSD) analysis of retinal field potentials. I. Methodological considerations and depth profiles. [Internet]. Journal of neurophysiology. 1994 Jul ;72(1):84-95.Available from: http://www.ncbi.nlm.nih.gov/pubmed/7965035
11. Thomas BB, Arai S, Ikai Y, Qiu G, Chen Z, Aramant RB, et al. Retinal transplants evaluated by optical coherence tomography in photoreceptor degenerate rats. [Internet]. Journal of neuroscience methods. 2006 Mar ;151(2):186-93.Available from: http://www.ncbi.nlm.nih.gov/pubmed/16129495
12. Huang Y, Cideciyan AV, Papastergiou GI, Banin E, Milam AH, Semple-Rowland SL, et al. Relation of optical coherence tomography to microanatomy in normal and rd chickens. [Internet]. Investigative ophthalmology & visual science. 1998 Nov ;39(12):2405-16.Available from: http://www.ncbi.nlm.nih.gov/pubmed/9804149
13. Metz S, Bertsch A, Bertrand D, Renaud P. Flexible polyimide probes with microelectrodes and embedded microfluidic channels for simultaneous drug delivery and multi-channel monitoring of bioelectric activity [Internet]. Biosensors & bioelectronics. 2004 ;19(10):1309-1318.Available from: http://www.ncbi.nlm.nih.gov/pubmed/15046764
14. McAdams E, Lackermeier A, McLaughlin JA, Macken D, Jossinet J. The linear and non-linear electrical properties of the electrode-electrolyte interface [Internet]. Biosensors and Bioelectronics. 1995 ;10(1-2):67-74.Available from: http://linkinghub.elsevier.com/retrieve/pii/095656639596795Z
15. Cole KS. Permeability and impermeability of cell membranes for ions [Internet]. Cold Spring Harbor Symposia on Quantitative Biology. 1940 Jan ;8110-122.Available from: http://symposium.cshlp.org/content/8/110.short
16. Grimnes S, Martinsen ØG. Bioimpedance and Bioelectricity Basics (Second Edition). Academic Press; 2008.
17. Mercanzini A, Colin P, Bensadoun J-C, Bertsch A, Renaud P. In vivo electrical impedance spectroscopy of tissue reaction to microelectrode arrays [Internet]. IEEE Transactions on Biomedical Engineering. 2009 ;56(7):1909-18.Available from: http://www.ncbi.nlm.nih.gov/pubmed/19362904
18. Zahn M. Electromagnetic Field Theory: A Problem Solving Approach. Second. Krieger Publishing Company; 2003.
19. Jacobs P, Varlan A, Sansen W. Design optimisation of planar electrolytic conductivity sensors [Internet]. Medical & biological engineering & computing. 1995 Nov ;33(6):802-10.Available from: http://www.ncbi.nlm.nih.gov/pubmed/8558953
20. Kern W. Handbook of Semiconductor Wafer Cleaning Technology - Science, Technology, and Applications. Elsevier Science and Technology Books; 1993.
21. Hagins WA, Penn RD, Yoshikami S. Dark current and photocurrent in retinal rods. [Internet]. Biophysical journal. 1970 ;10(5):380-412.Available from: http://www.ncbi.nlm.nih.gov/pubmed/5439318

22. Karwoski CJ, Frambach DA, Proenza LM. Laminar profile of resistivity in frog retina [Internet]. Journal of neurophysiology. 1985 Dec ;54(6):1607-19.Available from: http://www.ncbi.nlm.nih.gov/pubmed/3878863

23. Doh ST, Hao H, Loh SC, Patel T, Tawil HY, Chen DK, et al. Analysis of retinal cell development in chick embryo by immunohistochemistry and in ovo electroporation techniques. [Internet]. BMC developmental biology. 2010 Jan ;10(1):8.Available from: http://www.pubmedcentral.nih.gov/articlerender.fcgi?artid=2822752&tool=pmcentrez&rendertype=abstract

24. Livesey FJ, Cepko CL. Vertebrate neural cell-fate determination: lessons from the retina. [Internet]. Nature reviews. Neuroscience. 2001 Feb ;2(2):109-118.Available from: http://www.ncbi.nlm.nih.gov/pubmed/11252990

25. Sieving PA, Steinberg RH. Proximal retinal contribution to the intraretinal 8-Hz pattern ERG of cat. [Internet]. Journal of neurophysiology. 1987 Jan ;57(1):104-120.Available from: http://www.ncbi.nlm.nih.gov/pubmed/3559667